Journal of Colloid and Interface Science 575 (2020) 317–325

Contents lists available at ScienceDirect

Journal of Colloid and Interface Science

journal homepage: www.elsevier.com/locate/jcis

Polyamide-amine-epichlorohydrin (PAE) induced TiO_2 nanoparticles assembly in cellulose network

Vikram Singh Raghuwanshi *, Uthpala Manavi Garusinghe, Warren Batchelor, Gil Garnier *

Bioresource Processing Research Institute of Australia (BioPRIA), Department of Chemical Engineering, Monash University, Victoria 3800, Australia

GRAPHICAL ABSTRACT

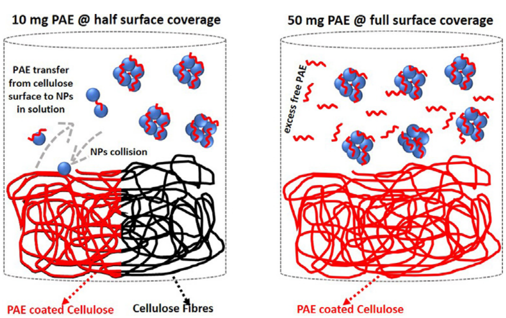

ARTICLE INFO

Article history:
Received 3 February 2020
Revised 27 April 2020
Accepted 27 April 2020
Available online 29 April 2020

Keywords:
Titanium dioxide (TiO_2)
Nanocellulose
Polyamide-amine-epichlorohydrin (PAE)
SEM
Small and Wide-Angle X-ray Scattering (SAXS/WAXS)

ABSTRACT

Hypothesis: TiO_2-NPs-Cellulose composites functionality depends on the retention and dispersion of NPs in the composites. SAXS and SEM can be combined to reveal the effect PAE has on the NPs aggregation, retention and interaction mechanisms in the composites.
Experiments: TiO_2-NPs-Cellulose sheets were made by first preparing PAE-cellulose suspensions of different PAE dosages (10 and 50 mg of PAE/g fibres). The TiO_2 NPs suspension (at different NPs loading) was then added to the cellulose-PAE suspension. The final suspension was used to make flexible paper-like composites sheets. SEM and SAXS quantified NPs retention and aggregation state.
Findings: PAE dosage of 20 mg/g cellulose provides full surface coverage of cellulose fibres. A 10 mg of PAE/g cellulose covers half the cellulose surface area and no free PAE remains in the suspension. PAE dosage of 50 mg/g cellulose gives full cellulose surface coverage and provides a large amount of PAE (30 mg/g cellulose) free in the suspension. Surprisingly, at both PAE dosages, NP coagulates and the size of the aggregates increase with NPs loading. Aggregates of two particle sizes (10 and 35 nm) are formed and the number density of smaller particles is higher than larger particle. The NPs aggregates and their retention are similar at both PAE dosages, which is explained by different PAE-NPs bridging mechanisms.

1. Introduction

TiO_2 nanoparticles (NPs) have a high surface area and a suitable band gap (≈3 eV) for photocatalysis, are non-toxic, transparent and chemically stable [1–4]. Composites with embedded TiO_2 NPs have emerged as functional materials for applications as photo-catalyst for solar energy conversion and dye degradation, and act antibacterial agent for air and water purification [5–8]. The interaction among NPs upon light exposure plays an important role in the functionality of the composites. The control and quantification of the NP aggregation state within the composite are critical [9].

* Corresponding author.
E-mail addresses: vikram.raghuwanshi@monash.edu (V.S. Raghuwanshi), gil.garnier@monash.edu (G. Garnier).

https://doi.org/10.1016/j.jcis.2020.04.121
0021-9797/

Applications fully utilizing TiO_2 NPs potential require an embedding network which keeps NPs functionality while preventing their leaching into the environment. Among the various materials, cellulose fibres and the non-woven composites made of those are very attractive for their renewable aspect, low cost and ease of manufacturing using the efficient papermaking process [10–12]. The composites produced are also thin and very flexible. The three –OH groups per glucosidic monomer forming the cellulose chain can directly interact with NPs or be easily chemically functionalized to retain NPs without losing their functionality [13]. Cellulose nanofibres of diameter 5–30 nm provide a high strength network of good optical transparency, large surface area, mechanical and thermal properties [14–17].

Since cellulose is a negatively charged polymer, retention aids are required to effectively hold anionic NPs in the cellulose fibres network. Cationic polyacrylamide (CPAM) and Polyamide-amine-epichlorohydrin (PAE) are commonly used in the paper industry as retention aid and wet-strength agent, respectively, [18,19]. Ngo et al. characterized the CPAM charge density effect on the aggregation state of gold NP and the resulting SERS amplification achieved [20]. CPAM, however, does not provide the wet strength required for the long use of composites under wet applications. PAE can be used as retention aid to flocculate NPs into aggregates of the desired size [21]. It is also a reactive bridging agent which strengthen the fibre-fibre bond in wet conditions [22,23]. PAE forms strong bonds with the cellulose through chemical cross linking at 105 °C [24,25].

The composites photocatalysis properties and applications depend on the good retention and dispersion of TiO_2 NPs in the cellulose fibre network while maintaining strength. Different PAE dosages affect the aggregation state, dispersion and retention of NPs in the cellulose network. It is expected that at low PAE dosages, PAE covers only a fraction of the cellulose fibre surface area available and the NPs are retained as individual particles (without NPs aggregation). However, at excess PAE dosages, providing the full surface coverage of cellulose fibres and leaving some excess polymer in solution, NPs are anticipated to retain as aggregates. The fundamental mechanisms by which the PAE dosage affects the TiO_2 NPs dispersion in cellulose composites and their respective photocatalysis properties are important for many applications but remain poorly understood.

X-rays scattering and electron microscopy are the two major characterisation technics which can reveal the internal and local structure as well as the composition of composites [34,35]. In particular, X-rays with wavelength in the angstrom scale are useful in determining changes in the atomic and nanometre dimensions [34]. Electron microscopy visualises the particles in the real space. However, the delicate sample preparation combined with the small area of view can create artefacts and provide misleading information. Small angle X-ray scattering (SAXS) is a non-destructive analytical method able to reveal structural information for particle size ranging from 1 to 100 nm [25–27]. In composites, SAXS can provide information on NPs shape, size, aggregates/assemblies formation, volume fraction, interparticle interactions and distribution of NPs over complete volume [26–28]. This extracted information will help in controlling and engineering the catalysis, photonic and structure dependent properties of specific composites.

To prove our hypothesis, the objective of this study is to quantify the retention level and aggregation state of TiO_2 NPs within the cellulose composites under controlled PAE concentration. The aggregation state and retention level of TiO_2 are quantified by SEM and SAXS methodology. Our aim is to establish the interaction mechanisms between TiO_2 NPs, PAE and the cellulose fibre network. Such capability is currently lacking to guide the efficient development of low cost- TiO_2 based paper solar panels and paper diagnostics. This knowledge gained will help to better engineer the photocatalytic functionality of TiO_2 based composites for water decontaminations, energy generation and antibacterial activities.

2. Experiments

2.1. Materials

Microfibrillated cellulose (MFC) at 25 wt% solid was purchased from DAICEL Chemical Industries Limited, Japan (grade Celish KY-100G). The MFC mean diameter is 73 nm and the aspect ratio of 100–150. Anatase titanium dioxide (TiO_2) nanoparticles (at 40 wt % solids) of average diameter 5–50 nm was purchased from US Research Nanomaterials, USA. Polyamide-amine-epichlorohydrin (PAE) was supplied by Nopco Paper Technology Pty Ltd, Australia.

2.2. TiO_2-cellulose composite sheets preparation

Composite sheets were prepared with a two-step process. In the first step, PAE suspension (10 mg or 50 mg/g MFC) was added into the 0.3 wt% (1.2 g fixed) MFC suspension at a constant flowrate of 30 mL/min by using a peristatic pump. While PAE is added, the cellulose-PAE suspension was stirred at high shear using an electric hand mixer (Kambrook Pty Ltd, Australia, model KSB8WHT). In the second step, the 0.1 wt% TiO_2 suspensions were pre-sonicated (Sonicator model VCX750; John Morris Scientific Pty Ltd) for 10 min at 80% amplitude. The sonicated TiO_2 suspension was added to the MFC-PAE suspension at a constant flowrate of 20 mL/min. Finally, the TiO_2-PAE-Cellulose suspension was poured into the British hand sheet maker (model T205) and the composite sheets were made. The prepared sheets were pressed at 385 kPa for 5 min and then dried at 105 °C. Detailed composite preparation method is provided in our previous article [22]. Composites with a fixed PAE dosage of 10 mg PAE/g MFC and with varying TiO_2 loadings of 0.5, 1, 2, 5, 10, 40 and 80 wt% were prepared with this method by varying the PAE concentration.

2.3. Scanning electron microscope (SEM)

Scanning electron micrograph (SEM) of the composite sheets were made using a FEI Magellan 400 FEGSEM. Samples were cut into 3 mm × 3 mm mounted onto a metal sample holder and coated with a thin layer of Iridium prior to imaging.

2.4. Small and Wide-angle X-ray scattering (SAXS/WAXS)

SAXS/WAXS measurements were performed at the SAXS/WAXS beamline of the Australian Synchrotron, Australia [29]. SAXS/WAXS measurements were made at the energy of 12 keV (λ = 1.033 Å) at three sample to detector distances covering the q range between ~0.001 to 0.2 $Å^{-1}$. The scattered photons from the sample were collected using PILATUS 1 M detector (pixel size 70 µm × 70 µm). Silver behenate was used to calibrate the q values. Scattering curves were normalized to the absolute scattering cross section by using the scattering curve of the glassy carbon. The final scattering curves were extracted after the data reduction and radial averaging using the beamline specific *ScatterBrain* software.

3. Results

3.1. SEM micrographs

Scanning electron microscopy (SEM) provides the real space images of TiO_2 NPs retention and aggregation in the cellulose network at low (10 mg/g MFC) and high (50 mg/g MFC) PAE dosages.

For the low PAE dosage and at 1 wt% NPs loading, the TiO_2 particles adsorb as singlets and only a few small NP aggregates are observed (Fig. 1a). At a higher NPs loading of 5 wt%, larger aggregates start forming (Fig. 1b). The size of these aggregates increases with increasing NPs loading until 80 wt% (Fig. 1c and d). NPs retention increases with the loading of NPs in the cellulose network.

SEM micrographs of composites made with high (50 mg/g MFC) and low (10 mg/g MFC) PAE dosage with 40 wt% and 80 wt% NPs loading are compared (Fig. 1e and f). At both PAE dosages, micrographs of composites made with 40 wt% NPs show similar NP distributions. However, composites loaded with 80 wt% NPs at the high PAE dosage form and retain larger NPs agglomerates compared to those made at low PAE dosage (Fig. 1f). SEM provides only a local surface area map within a few micrometres depth. It is difficult with SEM to generate the complete information describing the NPs retention, distribution and inter-particles interactions over a significant and representative sample volume.

3.2. SAXS curves analysis

Small angle X-ray scattering (SAXS) measurements were performed to extract TiO_2 NPs (1–80 wt%) retention and estimate the interparticle interactions for composites made at both the high and low PAE dosages (Fig. 2a–d). SAXS is a non-destructive method which provides a representative average value of the NPs shape, size, distribution and inter-particle interactions over a larger volume [30–32]. SAXS curves for TiO_2 NPs loading (for low PAE dosage) of up to 2 wt% have a similar shape with a broad hump seen between q = 0.02 and 0.06 $Å^{-1}$ (Fig. 2a). For the higher NPs loading (>5 wt%), the SAXS curves show three pronounced ordered peaks at q_1 = 0.011 $Å^{-1}$, q_2 = 0.022 $Å^{-1}$ and q_3 = 0.033 $Å^{-1}$, respectively. The clarity of these peaks is seen in the Kratky plots (Fig. 2c). Multiple ordered peaks indicate the NPs are retained in a short-range arranged assembly. The peak positions are not affected by the NPs loading and become more pronounced at the higher NP concentrations. An increase in the SAXS curves intensity as increases the NPs loading (>5 wt%) reveals higher retention and volume fraction of NPs in the cellulose network.

At the high PAE dosage, the SAXS curves for composites up to 40 wt% NPs loading are similar to the scattering curves of those at low PAE dosage (supporting information S1). This result indicates the same level of NPs retention for composites up to 40 wt % NPs loading, and the NPs retention to be independent of PAE dosage. At 80 wt% NPs loading, the SAXS curves of composites at

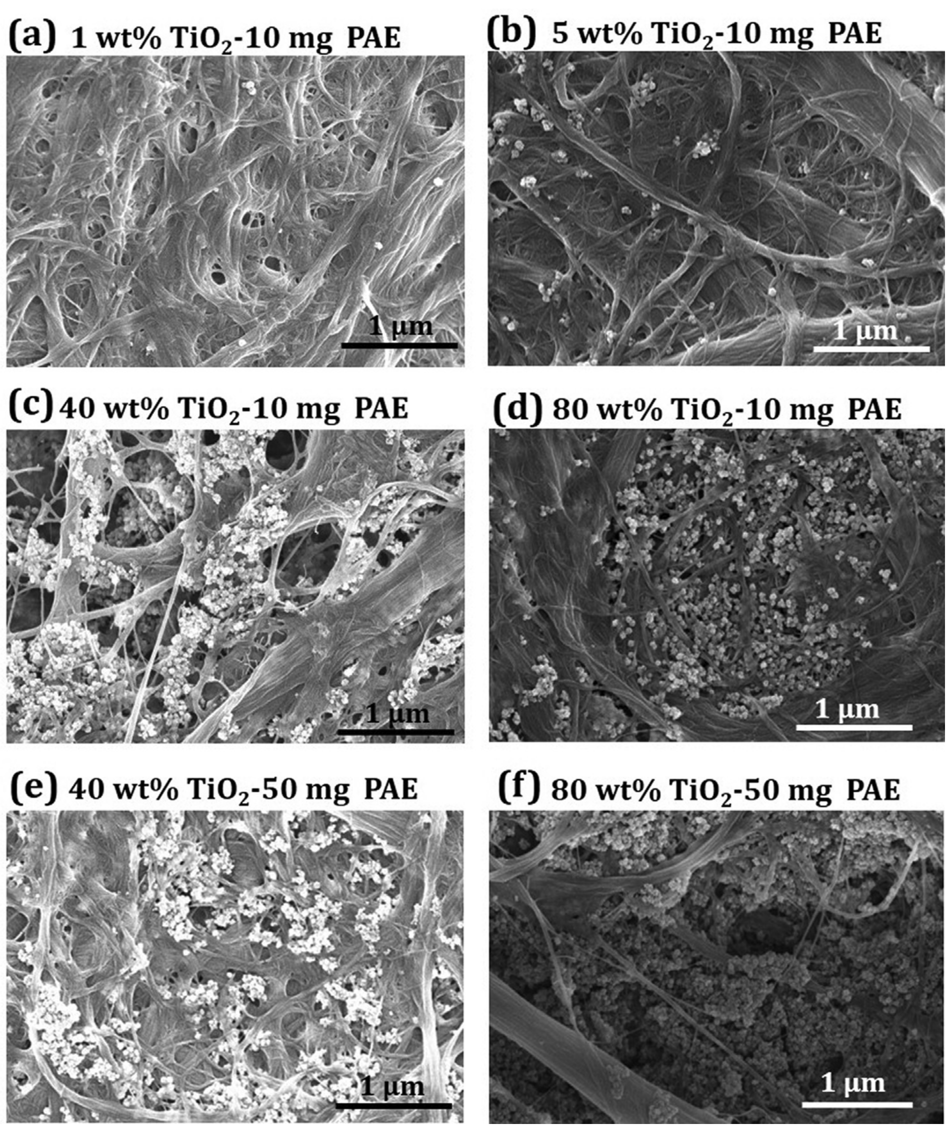

Fig. 1. SEM micrographs of TiO_2/PAE/cellulose composites made with different loadings of TiO_2 nanoparticles (1–80 wt%) retained with 10 mg of PAE/g MFC (a–d). TiO_2 NPs retained at 40 and 80 wt% loading with 50 mg of PAE/g cellulose (e–f).

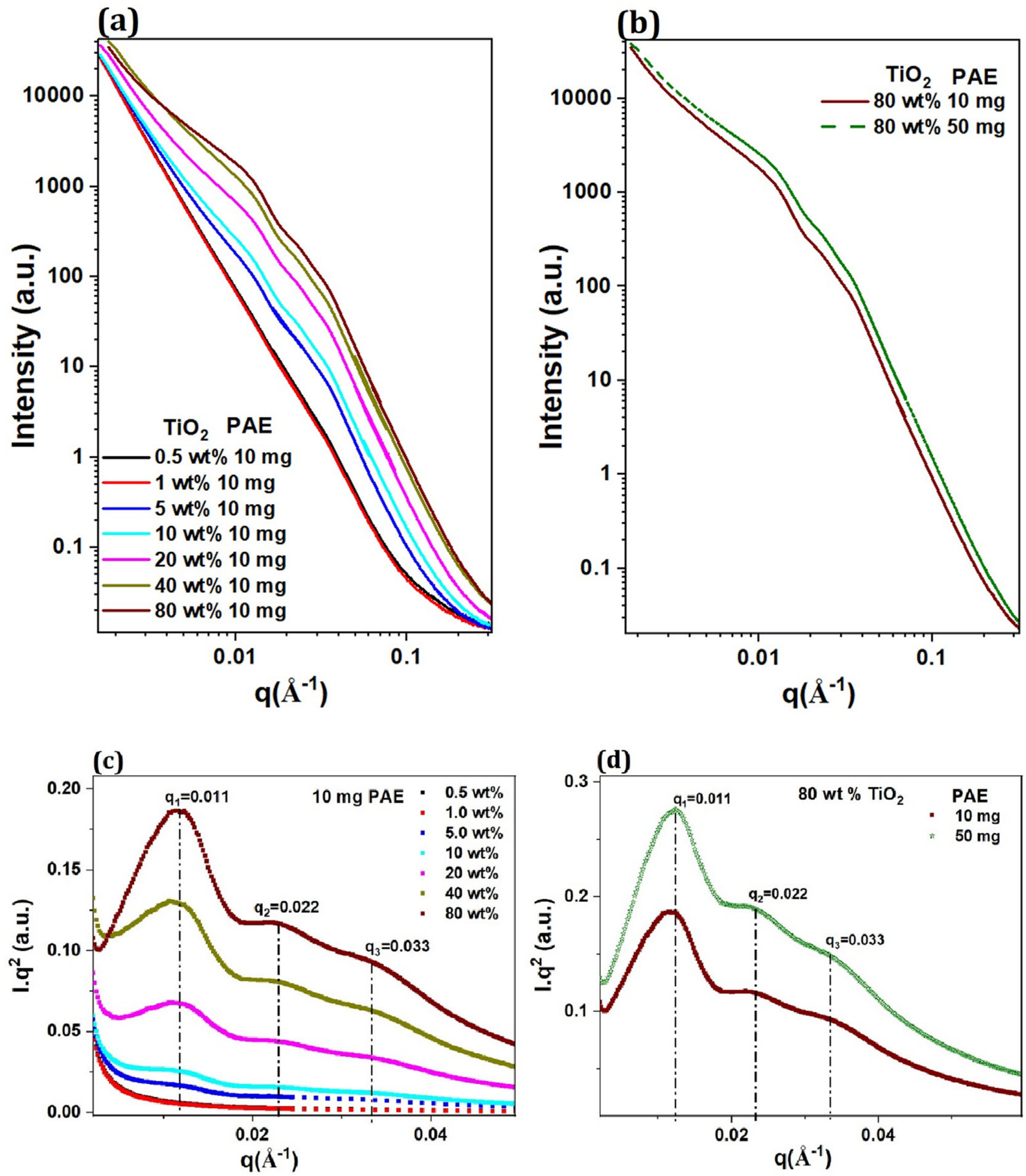

Fig. 2. (a) SAXS curves for composites made with 10 mg PAE/g cellulose and different TiO_2 NPs loading ranging from 0.5 wt% to 80 wt%. (b) SAXS curves comparison for the TiO_2 NPs retention at dosages of 10 and 50 mg PAE/g cellulose with 80 wt% NPs loading. (c) Kratky plot of the Fig (a). (d) Kratky plot of the Fig (b).

high and low PAE dosage show a similar shape (Fig. 2b). However, a high scattering intensity is observed for the composites with high PAE dosages which is seen clearly in the Kratky plots (Fig. 2d). The higher intensity indicates a higher amount of NPs retention at high PAE dosage compared to composites made at low PAE dosage.

The upturn in all the SAXS curves intensity below $q < 0.011$ Å^{-1} (Fig. 2a and b) shows the formation of larger size aggregates which is beyond the measured SAXS q range. Further information on particle shape, size distributions, correlation length, volume fraction and interparticle interaction is extracted from the SAXS curves by fitting with appropriate structure models. The analysis is presented below.

3.3. Information from SAXS curve fitting

The SAXS curves of composites made at the higher NPs loading (>5 wt%) are well fitted with the two spheres model and a lognormal distribution of particles. A structure factor of hard spheres surrounded by the similar type of particles was included in the fitting procedure. The fitted SAXS curves are provided in the supporting information (S2). The SAXS curves were fitted with a bimodal distribution of spheres (two sizes) with mean diameters of 10 nm and 35 nm, respectively (Fig. 3). The inset in Fig. 3 shows the distribution of the small particles (10 nm). These particles mixed and formed large assemblies of TiO_2 NPs in the cellulose network.

The structure factor (SF) obtained from the SAXS curves fitting reveals the interparticle interactions and volume fraction of the NPs retained in the cellulose network. The SF indicates how strongly the particles are interacting within the aggregates. No structure factor curve is observed for the TiO_2 NPs loading up to 2 wt%. The SF curves for the composites with TiO_2 NPs loading greater than 5 wt% at 10 mg PAE/g MFC dosage are shown in Fig. 4a. A broad single peak is observed for the sample loaded with 5 and 10 wt% TiO_2 NPs. Higher NPs loading (>20 wt%) shows 3 SF

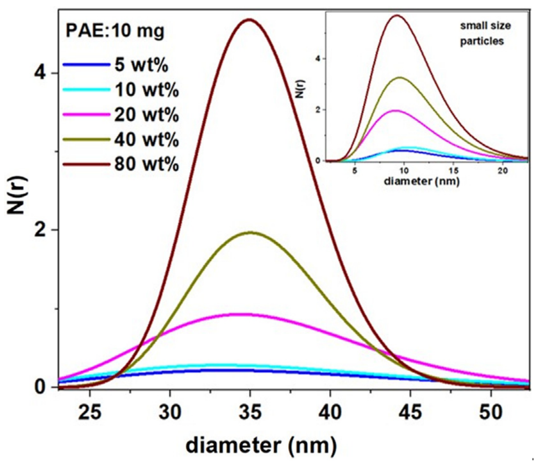

Fig. 3. Two spheres lognormal distributions obtained from SAXS curve fitting for the 10 mg PAE/g cellulose dosage and different TiO_2 NPs loadings ranging from 5 wt % to 80 wt%. Inset shows the distribution of small particles. The mean diameters are 10 nm (small) and 35 nm (large).

peaks at q = 0.011 $Å^{-1}$, 0.022 $Å^{-1}$ and 0.033 $Å^{-1}$. The peaks position remains at the same q values and does not change with higher NPs loading concentrations. However, the sharpness of the peak increases with loading, and the peaks are more pronounced. The SF peaks reveal that the NPs retained at the higher NPs loadings have stronger interparticle interactions compared to the NPs retained at the lower NPs loading.

The experimental volume fraction value for the TiO_2 NPs retained in the cellulose network with 10 mg PAE/g MFC is obtained from the SAXS curve fittings. The theoretical volume fraction is calculated by the mass and density of PAE (1.2 g/cm^3), cellulose (1.5 g/cm^3) and anatase TiO_2 NPs (3.8 g/cm^3) for different NPs loading wt%. The experimental and theoretical volume fractions are similar up to 40 wt% NPs loading (Fig. 4b). The mass fraction obtained from the ash test measurements [22] are in good comparison with the mass fraction calculated from the SAXS data analysis (supporting information S3). A significant difference in the volume fraction is obtained for the composites with 80 wt% NPs loading. At 80 wt% NPs loading, 60% of the NP's volume fraction is expected (calculated theoretically) to retain in the cellulose network. However, only half of the expected value of NPs volume fraction (30%) is retained in the cellulose network (Fig. 4b). This difference in volume fraction might be due to the loss of NP's retention at high NPs concentrations [33].

The correlation length provides the size of TiO_2 NPs assemblies in the cellulose network. Correlation length is evaluated from the full width and half maxima (FWHM) of the SF peaks at q = 0.011 $Å^{-1}$. The correlation length increases linearly from 150 nm (at 5 wt% NPs loading) up to 240 nm (for the 80 wt% NPs loading) at low PAE dosage (Fig. 5a). The number density obtained from the SAXS curves fitting for two different sizes is plotted as a function of TiO_2 NPs % loading for composites made at 10 mg of PAE/g MFC in Fig. 5b. Results indicate the number density of smaller size particles is dominating in the assemblies compared to the number density of large size particles.

3.4. Wide angle X-ray scattering (WAXS) curve analysis

WAXS experiment provides information on changes in the materials internal structure at the sub nanometre scale. In the composites, the WAXS measurement reveals variations in the crystallinity, degree of crystallinity and phases in the composite internal structure upon incorporating PAE and TiO_2 in the cellulose network. WAXS curves for composites with TiO_2 NPs loading ranging from 0.5 to 80 wt% for the 10 mg PAE/g MFC dosage are shown in Fig. 6a. The two broad peaks at q = 1.45 $Å^{-1}$ and 1.59 $Å^{-1}$ are from the cellulose structure which do not change with increase in NPs loading. This indicates the cellulose structure is unaffected by addition of PAE and TiO_2 NPs.

The peak at q = 1.78 $Å^{-1}$ appears from the [1 0 1] plane of TiO_2 [34]. The peak position remains the same for different NPs loading percent. The peak amplitude and the area under the peak increase significantly with increasing NPs loading wt% (Fig. 6b). Increase in the WAXS peak intensity and area indicate increase in the NPs retention amount in the [1 0 1] plane of TiO_2.

The WAXS curve were also compared for the TiO_2 80 wt% loading at high and low PAE dosages (inset Fig. 6a). At high PAE dosage, the peak at q = 1.78 $Å^{-1}$ shows higher scattering intensity indicating higher NPs retention amount than at low dosage.

4. Discussion

In this study, we engineer microfibrillated cellulose (MFC)-TiO_2 NP composites varying in NP content and assembly size. This was achieved by using 2 dosages of a polyelectrolyte and varying the NP addition level. The composites prepared are homogeneous,

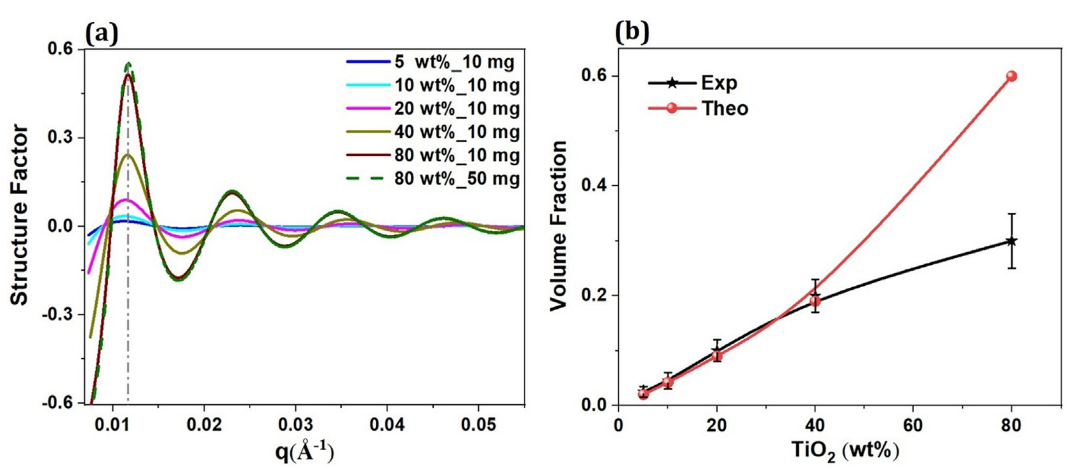

Fig. 4. (a) Structure factors evaluated after the SAXS curves fitting for composites with NPs loading ranging from 5 to 8 wt% at 10 mg PAE/g cellulose dosage. The dashed line shows the structure factor peak from composites loaded with 80 wt% NPs with a dosage of 50 mg PAE/g cellulose. (b) Theoretical and experimental calculated volume fractions of retained NPs at 10 mg PAE/g cellulose dosage.

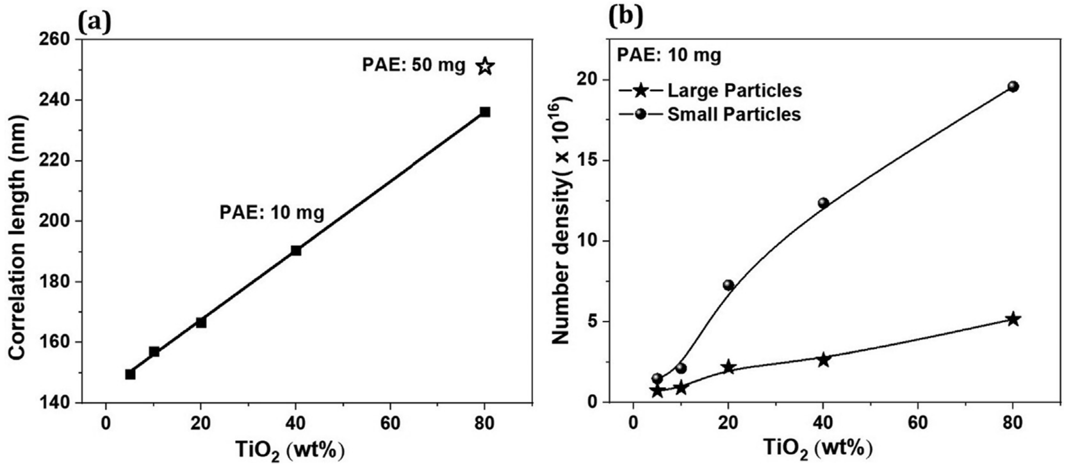

Fig. 5. (a) Correlation length calculated from the structure factor peaks for composites with PAE dosage 10 mg/g cellulose (TiO_2 NPs loading; 5–80 wt%) and 50 mg PAE/g cellulose dosage (80 wt% TiO_2 NPs loading). Solid line shows the linear fit. Open star symbol shows the correlation length of 80 wt% loaded NPs at PAE dosage of 50 mg/g cellulose. (b) Number density of the small and large size particles for 10 mg PAE/g cellulose dosages at different NPs loading from 5 to 80 wt%.

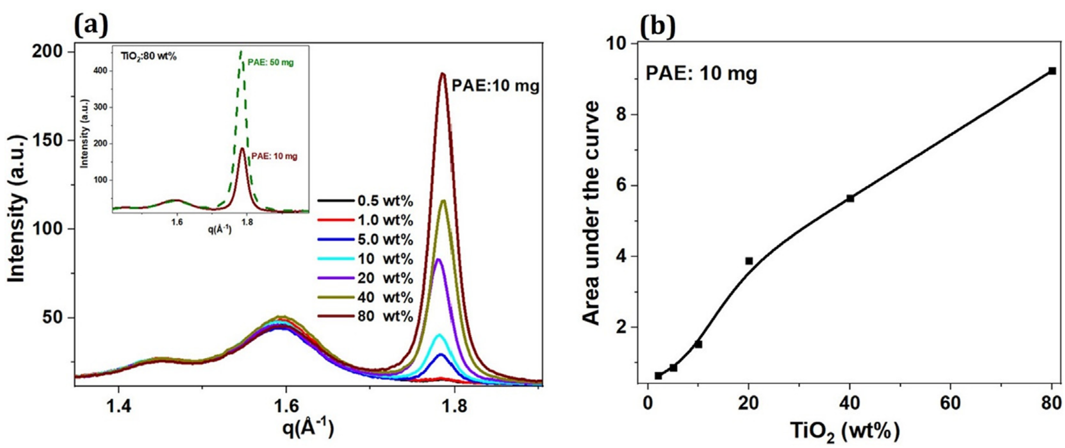

Fig. 6. a) WAXS curves for composites made at 10 mg PAE/g cellulose dosage and different TiO_2 NPs loading (0.5–80 wt%). The inset shows the comparison of WAXS curves of 80 wt% loaded NPs at 10 and 50 mg of PAE/g MFC dosage. (b) Plot of the area under the curve for different NPs loading wt% at 10 mg PAE/g MFC dosage. The area calculated for the peak represent the TiO_2 NPs at q = 1.78 $Å^{-1}$.

photocatalytic and remain strong when wet and their properties are reproducible [22]. The polyelectrolyte used is a polyamide-amine-epichlorohydrin (PAE) of molecular weight 200 kDa. The PAE monomer contains a cationic primary amide group (for retention) and an azetidinium function group for cross linking with the COOH groups by covalent bonds [35]. PAE has a high affinity for cellulose and is used as wet strength agent to maintain the integrity of cellulose fibrous structures in water.

TiO_2-cellulose composites were prepared by first mixing under high shear the wet strength/retention aid PAE with the cellulose nanofibre suspension. This was followed by addition of the TiO_2 NPs suspension. Both MFC and TiO_2 are anionic; therefore, a cationic polymer - PAE is used to retain NPs in the cellulose fibre network.

The zeta potential of the cellulose fibres and TiO_2 NPs are −26 mV and −11 mV, respectively. The low zeta potential of TiO_2 contributes to its natural tendency to form small aggregates in suspension. When 10 mg PAE/g is mixed with the cellulose fibres, the zeta potential of the suspension reverses and increases to +25 mV. For 50 mg PAE/g fibre, it becomes +40 mV. Positive value of zeta potential drives the adsorption of negatively charged TiO_2 onto the cellulose/PAE interface.

The surface area of MFC in all composites is ≈44 m^2 and was kept constant. The high PAE dosage of 50 mg/g of MFC was selected to provide full surface coverage (20 mg PAE/g MFC) of fibres and to leave a substantial excess in solution. The low PAE dosage of 10 mg of PAE/g fibre provides half surface coverage of MFC (≈22 m^2). It is associated with half the maximum coagulation rate, assuming a purely bridging mechanism. The adsorption isotherm of PAE adsorption onto cellulose fibres was published previously [22].

At low PAE dosage, no excess free PAE is expected in suspension prior to the addition of TiO_2 NP. This is because of the high affinity PAE has for cellulose and the low dosage used. Therefore, upon adding NPs, the highest retention of TiO_2 as individual particles onto MFC is expected. However, upon increasing TiO_2 NPs loading (>10 wt%), the NPs retained as large aggregates of high correlation lengths. This was not expected from a pure bridging mechanism. The formation of NP aggregates can be explained by some transfer of the low Mw PAE from the MFC surface to the NPs upon collision (Fig. 7 left).

The effect of shear induced polymer transfer on aggregation was previously analysed for CPAM of different molecular weight and charge densities [36]. Basically, the shear induced polymer transfer refers to the breaking-up of physical bonds between the adsorbed

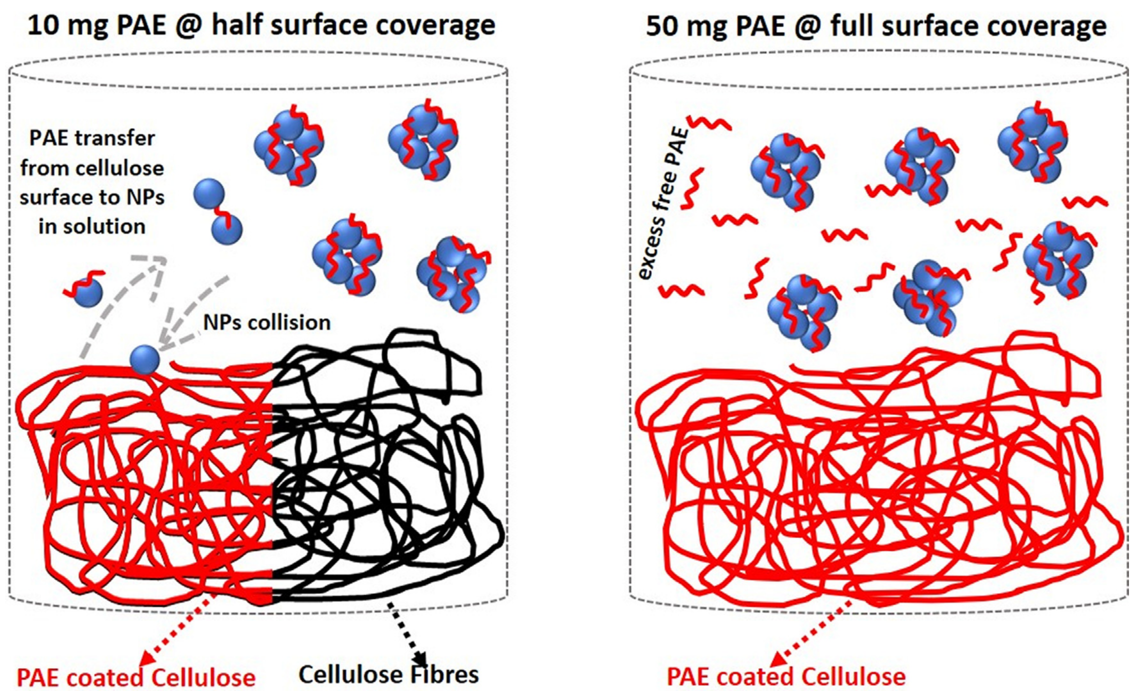

Fig. 7. Schematic of the TiO_2 NPs aggregation mechanisms for different PAE dosages; half cellulose surface coverage by 10 mg PAE/g MFC (Left) and full cellulose surface coverage with excess in solution by 50 mg PAE/g MFC (Right).

PAE and cellulose due to shear. High shear was applied during mixing TiO_2 NPs with the PAE-cellulose suspension. The shear desorbs some PAE molecules from the MFC surface upon collision of a NP. This partially PAE coated NP then aggregates with other NPs upon collision by a bridging or charge reversal mechanism. Accordingly to the charge reversal mechanism, the PAE adsorbed at the TiO_2-NPs interface reverses the NP's surface charge from negative to positive. This allows NPs to interact with other negatively charged NPs and to form aggregates by electrostatic interactions. These PAE-TiO_2 aggregates adsorb at the MFC surface by electrostatic attraction and retain in the network by filtration effect.

At high PAE dosage, 20 mg of PAE/g MFC is required to fully covers all the MFC fibres surface. The remaining 30 mg PAE remains as an excess polymer in solution (Fig. 7 right). Upon loading different content (wt%) of TiO_2 NPs, the excess PAE directly adsorbs onto the NPs to form large aggregates mostly by bridging. At the highest NPs loading, the size of the aggregates formed is 250 nm which is comparable to that formed at low PAE dosage (230 nm). The NPs aggregates later adsorb at the MFC surface or retained within the fibrous structure upon eliminating shear for composite making.

At low NPs loadings up to 2 wt% (at both PAE dosages)- SEM micrographs show fewer NPs retention as small aggregates (Fig. 1a). Increasing NPs loading (up to 80 wt%) increases the retention of NPs and forms large aggregates in the cellulose network (Fig. 1c and d). Both PAE dosages show a similar retention of NPs in the cellulose network (Fig. 1c–f).

At both PAE dosages, SAXS curves of TiO_2 loading up to 2 wt% show a dominating scattering from the large-scale heterogeneities of cellulose fibre aggregates and their distribution. However, for the higher NPs loading (>5 wt%), ordered peaks at q = 0.011 $Å^{-1}$, q = 0.022 $Å^{-1}$ and q = 0.033 $Å^{-1}$ reveal the retained NPs in the cellulose network. The peak positions indicate that the NPs are arranged in a short range ordered aggregates (Fig. 2c). The NPs aggregates are composed of a bimodal distribution of particle of sizes 10 and 35 nm. In these aggregates, the number density of smaller size particles is in excess compared to the big size particles (Fig. 5b). The broad structure factor peaks up to 10 wt% NPs loading shows weak interparticle interaction in the NPs aggregates. However, high NPs loading (>20 wt%) increases the interparticle interactions within aggregates.

For composites up to 40 wt% NPs loading (at both PAE dosage), the SAXS curves show the same scattering profile, revealing similar retention of NPs for composites. Previously, ash test confirmed the retention of NPs to be independent of PAE dosage up to a loading of TiO_2 up to 40 wt% [22]. However, SAXS/WAXS curves for composites at 80 wt% loading and 50 mg PAE/g MFC dosage show a slightly higher scattering intensity revealing higher NPs retention than those at 10 mg PAE/g MFC (Figs. 6a and 2d).

At both PAE dosages, NPs retention increases with increasing NP loading concentration. Interestingly, no structure difference is found in the TiO_2 NPs aggregate sizes and retention on the MFC surface. The similar NPs retention is due to application of different retention mechanisms at low and high PAE dosages. At low PAE dosage, the NPs aggregates are formed and retained by PAE transferred from the MFC surface. However, at high PAE dosage, the NPs aggregate due to the excess PAE in the suspension. At both PAE dosages, NPs aggregate by PAE induced bridging and charge reversal mechanism.

5. Conclusion

A series of TiO_2-Nanocellulose composites varying in nanoparticle (NP) content and aggregation size was created and characterized with an advanced SAXS method. PAE was successfully used as strength agent and retention aid to control the TiO_2 NPs distribution in the cellulose fibre network. Flexible cellulose/TiO_2 NPs paper composites were made with different NP (0.5–80%) loadings at two PAE dosages corresponding to half cellulose coverage (10 mg/g cellulose) and full coverage with excess in suspension (50 mg/g cellulose).

At both PAE dosages, SEM and SAXS analysis show the NPs retention and aggregate size to increase with the NPs loading in the cellulose network. The aggregates are made of two NP sizes

(10 and 35 nm) and exhibit a higher number density of the small particles than the large particles. The broad structure factor peaks reveal weak interparticle interaction in the NPs aggregates (up to 10 wt%). However, the interparticle interactions within aggregates becomes stronger at high NPs loading (>20 wt%). WAXS measurements prove that PAE and TiO_2 addition has no effect on the cellulose nanostructure and only the NPs retention increases with increasing NPs loading.

Similar NPs retention are measured in the cellulose network at both PAE dosages; this is explained by different PAE-NPs interaction mechanisms [37]. At low PAE dosage, all PAE adsorbs onto cellulose and no free PAE remains in the suspension when the NP are added. The NPs aggregate by shear induced PAE transfer from cellulose to TiO_2 particles by a combination of bridging and charge reversal mechanism [38]. However, at high dosages, PAE completely covers the cellulose fibres with an important excess of PAE in suspension. This excess PAE aggregates NPs via a bridging mechanism.

This study characterized in fine detail the nanoparticle retention and controlled aggregation in paper-like nanocellulose- TiO_2 NPs composites using PAE, a polyelectrolyte providing the material its wet strength. This is because TiO_2 distribution in a material affects its photocatalysis [39–41]. SAXS/WAXS provide NPs retention, distribution and NPs-PAE-cellulose interaction mechanisms at the nanometer and atomic scales, completing electron microscopy characterizing the micro scale [40,42]. The PAE induced NPs aggregation and retention in the cellulose network allow engineering highly efficient and functional TiO_2 NPs cellulosic composites for catalytic applications.

CRediT authorship contribution statement

Vikram Singh Raghuwanshi: Investigation, Data curation,Formal analysis, Writing-original draft. **Uthpala Manavi Garusinghe:** Investigation, Data curation. **Warren Batchelor:** Writing-review and editing. **Gil Garnier:** Writing-original draft, Formal analysis, Writing-review & editing.

Declaration of Competing Interest

The authors declare that they have no known competing financial interests or personal relationships that could have appeared to influence the work reported in this paper.

Acknowledgement

Financial support is from Australian Research Council (ARC), Australian paper, Norske Skog, Orora and Visy through the Industry Transformation Research Hub grant IH130100016. Many thanks to The Australian Synchrotron for beam time.

Appendix A. Supplementary material

Supplementary data to this article can be found online at https://doi.org/10.1016/j.jcis.2020.04.121.

References

[1] M. Auffan, J. Rose, J.Y. Bottero, G.V. Lowry, J.P. Jolivet, M.R. Wiesner, Towards a definition of inorganic nanoparticles from an environmental, health and safety perspective, Nat. Nanotechnol. 4 (2009) 634–641.

[2] C. Sanchez, P. Belleville, M. Popall, L. Nicole, Applications of advanced hybrid organic-inorganic nanomaterials: from laboratory to market, Chem. Soc. Rev. 40 (2011) 696–753.

[3] M.R. Ranade, A. Navrotsky, H.Z. Zhang, J.F. Banfield, S.H. Elder, A. Zaban, P.H. Borse, S.K. Kulkarni, G.S. Doran, H.J. Whitfield, Energetics of nanocrystalline TiO_2, P. Natl. Acad. Sci. USA 99 (2002) 6476–6481.

[4] M. Dahl, Y. Liu, Y. Yin, Composite titanium dioxide nanomaterials, Chem. Rev. 114 (2014) 9853–9889.

[5] J.W. Rhim, H.M. Park, C.S. Ha, Bio-nanocomposites for food packaging applications, Prog. Polym. Sci. 38 (2013) 1629–1652.

[6] E. Bet-moushoul, Y. Mansourpanah, K. Farhadi, M. Tabatabaei, TiO_2 nanocomposite based polymeric membranes: a review on performance improvement for various applications in chemical engineering processes, Chem. Eng. J. 283 (2016) 29–46.

[7] H. Choi, A. Zakersalehi, S.R. Al-Abed, C. Han, D.D. Dionysiou, Chapter 8 - nanostructured titanium oxide film- and membrane-based photocatalysis for water treatment, in: A. Street, R. Sustich, J. Duncan, N. Savage (Eds.), Nanotechnology Applications for Clean Water (Second Edition), William Andrew Publishing, Oxford, 2014, pp. 123–132.

[8] A. Sodagar, M.S.A. Akhoundi, A. Bahador, Y.F. Jalali, Z. Behzadi, F. Elhaminejad, A.H. Mirhashemi, Effect of TiO_2 nanoparticles incorporation on antibacterial properties and shear bond strength of dental composite used in Orthodontics, Dental Press J. Orthod. 22 (2017) 67–74.

[9] F. Pellegrino, L. Pellutie, F. Sordello, C. Minero, E. Ortel, V.D. Hodoroaba, V. Maurino, Influence of agglomeration and aggregation on the photocatalytic activity of TiO_2 nanoparticles, Appl. Catal. B-Environ. 216 (2017) 80–87.

[10] K. Bethke, S. Palantoken, V. Andrei, M. Ross, V.S. Raghuwanshi, F. Kettemann, K. Greis, T.T.K. Ingber, J.B. Stuckrath, S. Valiyaveettil, K. Rademann, Functionalized cellulose for water purification, antimicrobial applications, and sensors, Adv. Funct. Mater. 28 (2018) 1800409.

[11] D. Klemm, B. Heublein, H.P. Fink, A. Bohn, Cellulose: fascinating biopolymer and sustainable raw material, Angew. Chem. Int. Ed. 44 (2005) 3358–3393.

[12] R.J. Moon, A. Martini, J. Nairn, J. Simonsen, J. Youngblood, Cellulose nanomaterials review: structure, properties and nanocomposites, Chem. Soc. Rev. 40 (2011) 3941–3994.

[13] V.S. Raghuwanshi, J. Su, C.J. Garvey, S.A. Holt, P.J. Holden, W.J. Batchelor, G. Garnier, Visualization and quantification of IgG antibody adsorbed at the cellulose-liquid interface, Biomacromolecules 18 (2017) 2439–2445.

[14] D. Klemm, F. Kramer, S. Moritz, T. Lindstrom, M. Ankerfors, D. Gray, A. Dorris, Nanocelluloses: a new family of nature-based materials, Angew. Chem. Int. Ed. 50 (2011) 5438–5466.

[15] Y. Habibi, Key advances in the chemical modification of nanocelluloses, Chem. Soc. Rev. 43 (2014) 1519–1542.

[16] A. Dufresne, Nanocellulose: a new ageless bionanomaterial, Mater. Today 16 (2013) 220–227.

[17] B. Thomas, M.C. Raj, K.B. Athira, M.H. Rubiyah, J. Joy, A. Moores, G.L. Drisko, C. Sanchez, Nanocellulose, a versatile green platform: from biosources to materials and their applications, Chem. Rev. 118 (2018) 11575–11625.

[18] M.A. Hubbe, H. Nanko, M.R. McNeal, Retention aid polymer interactions with cellulosic surfaces and suspensions: a review, Bioresources 4 (2009) 850–906.

[19] S.H. Yoon, X.S. Chai, Retention rate phenomena for polyamide-epichorohydrin polymer in papermaking fibrous colloidal suspension, J. Ind. Eng. Chem. 13 (2007) 237–243.

[20] Y.H. Ngo, D. Li, G.P. Simon, G. Garnier, Effect of cationic polyacrylamides on the aggregation and SERS performance of gold nanoparticles-treated paper, J. Colloid Interf. Sci. 392 (2013) 237–246.

[21] S. Varanasi, Z.X. Low, W. Batchelor, Cellulose nanofibre composite membranes - Biodegradable and recyclable UF membranes, Chem. Eng. J. 265 (2015) 138–146.

[22] U.M. Garusinghe, V.S. Raghuwanshi, W. Batchelor, G. Garnier, Water resistant cellulose - titanium dioxide composites for photocatalysis, Sci. Rep. 8 (2018) 2306.

[23] T. Obokata, A. Isogai, Effects of polyamideamine-epichlorohydrin (PAE) resin deterioration on PAE retention and wet strength performance in handsheet making, Appita J. 57 (2004) 411–414.

[24] T. Obokata, A. Isogai, The mechanism of wet-strength development of cellulose sheets prepared with polyamideamine-epichlorohydrin (PAE) resin, Colloid Surface A 302 (2007) 525–531.

[25] J. Su, W.K.J. Mosse, S. Sharman, W. Batchelor, G. Garnier, Paper strength development and recyclability with polyamideamine-epichlorohydrin (PAE), Bioresources 7 (2012) 913–924.

[26] V.S. Raghuwanshi, G. Garnier, Characterisation of hydrogels: linking the nano to the microscale, Adv. Colloid Interf. Sci. 274 (2019) 102044.

[27] P.S. Bauer, H. Amenitsch, B. Baumgartner, G. Koberl, C. Rentenberger, P.M. Winkler, In-situ aerosol nanoparticle characterization by small angle X-ray scattering at ultra-low volume fraction, Nat. Commun. 10 (2019) 1122.

[28] Y. Zhao, K. Thorkelsson, A.J. Mastroianni, T. Schilling, J.M. Luther, B.J. Rancatore, K. Matsunaga, H. Jinnai, Y. Wu, D. Poulsen, J.M.J. Frechet, A.P. Alivisatos, T. Xu, Small-molecule-directed nanoparticle assembly towards stimuli-responsive nanocomposites, Nat. Mater. 8 (2009) 979–985.

[29] N.M. Kirby, S.T. Mudie, A.M. Hawley, D.J. Cookson, H.D.T. Mertens, N. Cowieson, V. Samardzic-Boban, A low-background-intensity focusing small-angle X-ray scattering undulator beamline, J. Appl. Crystallogr. 46 (2013) 1670–1680.

[30] V.S. Raghuwanshi, U.M. Garusinghe, P. Raj, N. Kirby, A. Hoell, W. Batchelor, G. Garnier, Cationic polyacrylamide induced nanoparticles assembly in a cellulose nanofiber network, J. Colloid Interf. Sci. 529 (2018) 180–186.

[31] V.S. Raghuwanshi, U.M. Garusinghe, J. Ilaysky, W.J. Batchelor, G. Gamier, Effect of nanoparticles size and polyelectrolyte on nanoparticles aggregation in a cellulose fibrous matrix, J. Colloid Interf. Sci. 510 (2018) 190–198.

[32] O. Glatter, O. Kratky, Small-Angle X-Ray Scattering, Academic Press, London, 1982.

[33] C. Wang, A.D. Bobba, R. Attinti, C.Y. Shen, V. Lazouskaya, L.P. Wang, Y. Jin, Retention and transport of silica nanoparticles in saturated porous media: effect of concentration and particle size, Environ. Sci. Technol. 46 (2012) 7151–7158.

[34] A. Lamberti, A. Chiodoni, N. Shahzad, S. Bianco, M. Quaglio, C.F. Pirri, Ultrafast room-temperature crystallization of TiO_2 nanotubes exploiting water-vapor treatment, Sci. Rep. 5 (2015) 7808.

[35] T. Obokata, M. Yanagisawa, A. Isogai, Characterization of polyamideamine-epichlorohydrin (PAE) resin: Roles of azetidinium groups and molecular mass of PAE in wet strength development of paper prepared with PAE, J. Appl. Polym. Sci. 97 (2005) 2249–2255.

[36] T. Asselman, G. Garnier, Mechanism of polyelectrolyte transfer during heteroflocculation, Langmuir 16 (2000) 4871–4876.

[37] A. Azetsu, H. Koga, L.Y. Yuan, T. Kitaoka, Direct synthesis of gold nanocatalysts on TEMPO-oxidized pulp paper containing aldehyde groups, Bioresources 8 (2013) 3706–3717.

[38] L.L. Feng, M.C. Stuart, Y. Adachi, Dynamics of polyelectrolyte adsorption and colloidal flocculation upon mixing studied using mono-dispersed polystyrene latex particles, Adv. Colloid Interf. Sci. 226 (2015) 101–114.

[39] I. Chauhan, P. Mohanty, In situ decoration of TiO_2 nanoparticles on the surface of cellulose fibers and study of their photocatalytic and antibacterial activities, Cellulose 22 (2015) 507–519.

[40] A. Snyder, Z.Y. Bo, R. Moon, J.C. Rochet, L. Stanciu, Reusable photocatalytic titanium dioxide-cellulose nanofiber films, J. Colloid Interf. Sci. 399 (2013) 92–98.

[41] J. Zhang, W.X. Liu, P.P. Wang, K.F. Qian, Photocatalytic behavior of cellulose-based paper with TiO_2 loaded on carbon fibers, J. Environ. Chem. Eng. 1 (2013) 175–182.

[42] P. Hernandez-Cerdan, B.W. Mansel, A. Leis, L. Lundin, M.A.K. Williams, Structural analysis of polysaccharide networks by transmission electron microscopy: comparison with small-angle X-ray scattering, Biomacromolecules 19 (2018) 989–995.